International Journal of Nanomedicine

Dovepress
Taylor & Francis Group

Open Access Full Text Article

ORIGINAL RESEARCH

Boron Phenylalanine-Modified Polydopamine Nanoparticles for Targeted Delivery of Danusertib in Non-Small Cell Lung Cancer

Yi Xu[1,*], Xiang Chen[2,*], Lin Zhang[3], Ping Li[3], Jiahuan He[3], Meiyu Zhu[3], Pooyan Makvandi[4], Xuru Jin[2,3]

[1]Department of Urology, The Quzhou Affiliated Hospital of Wenzhou Medical University, Quzhou People's Hospital, Quzhou, Zhejiang, 324000, People's Republic of China; [2]Department of Respiratory and Critical Care Medicine, The First Affiliated Hospital of Wenzhou Medical University, Wenzhou, Zhejiang, 325000, People's Republic of China; [3]Department of Respiratory and Critical Care Medicine, The Quzhou Affiliated Hospital of Wenzhou Medical University, Quzhou People's Hospital, Quzhou, Zhejiang, 324000, People's Republic of China; [4]Zhejiang Provincial Research & Engineering Center for Endoscopic Instrument, Department of Science & Technology, The Quzhou Affiliated Hospital of Wenzhou Medical University, Quzhou People's Hospital, Quzhou, Zhejiang, 324000, People's Republic of China

*These authors contributed equally to this work

Correspondence: Xuru Jin, Department of Respiratory and Critical Care Medicine, The First Affiliated Hospital of Wenzhou Medical University, Shangcai Village, Nanbaixiang, Ouhai District, Wenzhou, Zhejiang, 325000, People's Republic of China, Tel +86-13857782369, Email xuru.jin@wmu.edu.cn; Pooyan Makvandi, Zhejiang Provincial Research & Engineering Center for Endoscopic Instrument, Department of Science & Technology, The Quzhou Affiliated Hospital of Wenzhou Medical University, Quzhou People's Hospital, Quzhou, Zhejiang, 324000, People's Republic of China, Email Pooyan.Makvandi@wmu.edu.cn

Purpose: Aurora-A is often overexpressed in lung cancer and is associated with poor prognosis, making it a potential therapeutic target for non-small cell lung cancer (NSCLC) treatment. This study aimed to evaluate the therapeutic potential of nanomedicine-based delivery of the Aurora-A inhibitor Danusertib (Danu) in NSCLC treatment.

Methods: Boron phenylalanine (BPA)-modified polydopamine (PDA) was used as a carrier to load Danu, preparing B-PDA@Danu nanoparticles. The structure, microstructure, particle size, zeta potential, stability, drug loading capacity, loading rate, and in vitro release were characterized. In vitro studies investigated its effects on A549 cell viability, apoptosis, uptake ability, and cell cycle. In vivo studies examined its distribution and/or anti-tumor effects in subcutaneous xenograft tumors in mice. The anti-tumor effects and biosafety of B-PDA@Danu were studied in a subcutaneous xenograft tumor model in mice. The in vivo distribution and anti-tumor effects of B-PDA@Danu were studied in a mouse lung carcinoma in situ model.

Results: The synthesized B-PDA@Danu nanoparticles were spherical, negatively charged, with an average particle size of (172.96 ±1.61) nm, exhibited good stability, and efficiently loaded Danu. B-PDA@Danu promoted cellular uptake in vitro, inhibited cell viability ($P < 0.001$), induced G2/M cell cycle arrest ($P < 0.001$), and increased apoptosis ($P < 0.001$). In the subcutaneous xenograft tumor model, B-PDA@Danu suppressed tumor growth ($P < 0.001$), induced cell cycle arrest in tumor cells ($P < 0.001$), caused tumor tissue damage, and showed good biosafety. In the mouse lung carcinoma in situ model, B-PDA@Danu effectively targeted and accumulated at the site of carcinogenesis, leading to tumor shrinkage.

Conclusion: B-PDA@Danu provides a novel nanomedicine approach for anti-NSCLC therapy that enables targeted tumor elimination with low potential toxicity.

Keywords: boron phenylalanine, polydopamine, Danusertib, non-small cell lung cancer

Introduction

The 2020 GLOBOCAN report revealed that lung cancer ranks second globally in terms of new cases and first in terms of mortality among human cancers.[1] Non-small cell lung cancer (NSCLC) constitutes the primary histological type of lung cancer, representing over 85% of all cases.[2] Current clinical approaches for NSCLC treatment typically encompass surgical resection, radiotherapy, chemotherapy, and immunotherapy, among others.[3] However, due to delayed diagnoses leading to metastasis or advanced stages, some patients lose the opportunity for surgical intervention.[3] Moreover, the

Received: 26 January 2025
Accepted: 17 June 2025
Published: 28 June 2025

Graphical Abstract

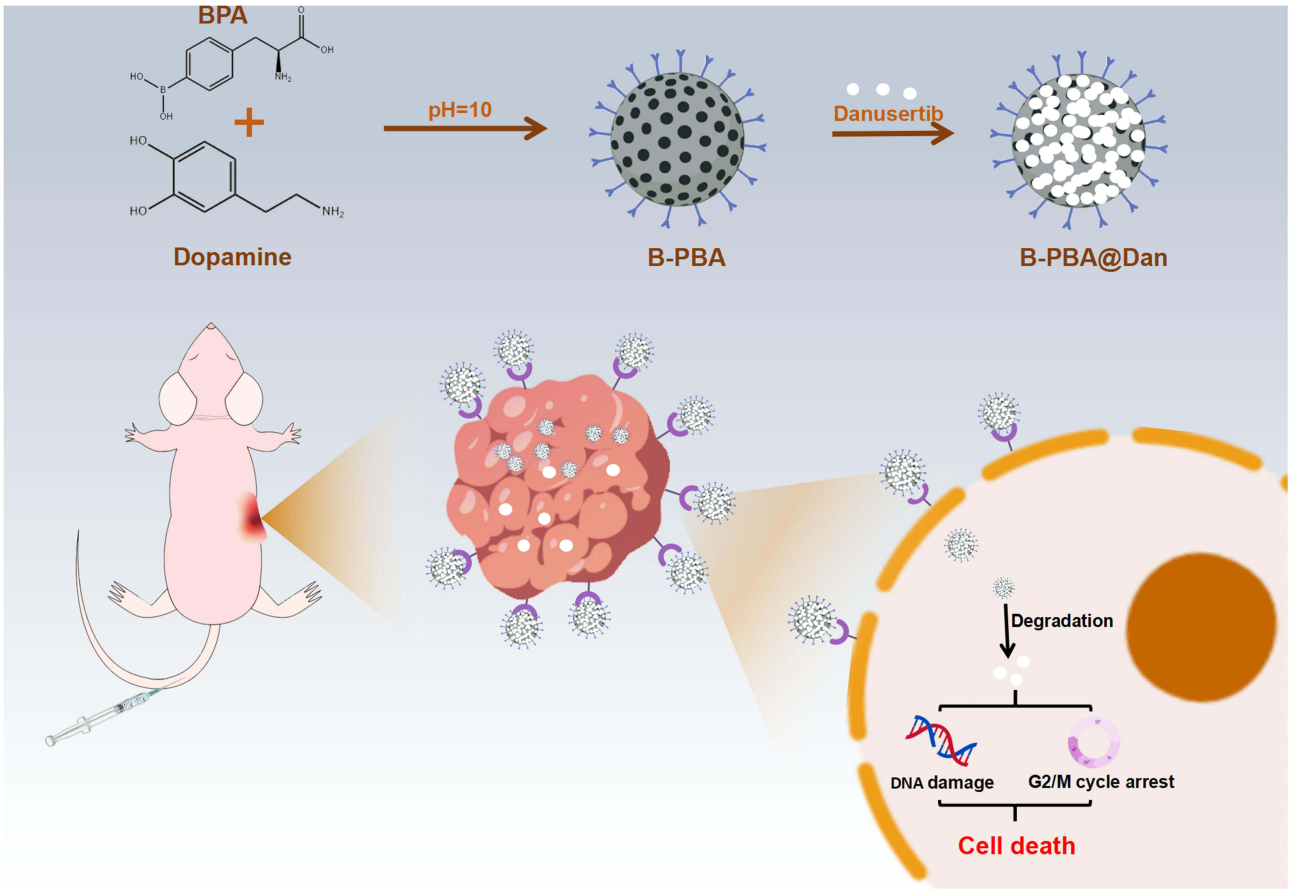

non-specific adverse effects associated with chemotherapy often subject patients to significant physical and psychological distress, sometimes hindering treatment adherence.[3] Consequently, the outlook for NSCLC treatment appears challenging, underscoring the urgent need for more precise and efficient targeted therapeutic agents to enhance cure rates and quality of life for NSCLC patients.

In normal cells, Aurora-A plays a crucial role in a series of key mitotic events and is one of the primary regulatory factors of the cell cycle.[4] However, in various human cancer types, Aurora-A promotes tumorigenesis through amplification and/or overexpression, including NSCLC, hepatocellular carcinoma, bladder cancer, colorectal cancer, and breast cancer, and is associated with poor prognosis.[4–7] Notably, studies indicate that inhibiting Aurora-A can lead to spindle formation abnormalities and mitotic defects, ultimately resulting in tumor cell death.[4–7] Therefore, Aurora-A may serve as a critical therapeutic target in NSCLC. Danusertib (Danu), a broad-spectrum Aurora-A inhibitor, has undergone clinical trials and demonstrated certain anti-tumor effects in multiple cancer types, establishing it as an effective Aurora-A inhibitor.[8,9] Despite showing promise as an anticancer agent, Danu still faces challenges in targeting efficiency and tolerability during clinical application. A growing body of research indicates that nanotechnology-based precision targeted therapy for lung cancer can minimize drug toxicity and enhance drug delivery to tumor sites, increasing drug accumulation within tumors, and improving treatment efficacy.[10,11] This has become an effective means to address the limitations of traditional targeted therapies. Hence, developing a nanodrug delivery system based on Danu for achieving targeted therapy holds great promise for improving survival rates and prognosis for NSCLC patients.

Various nanocarrier platforms, including liposomes, hydrogels, micelles, and nanoparticles, have been explored for drug delivery in cancer therapy. Liposomes, as phospholipid bilayer vesicles, offer biocompatibility and efficient encapsulation of hydrophilic and hydrophobic drugs, but they often suffer from limited structural stability and rapid clearance in vivo.[12] Hydrogels provide excellent drug retention and controlled release profiles, yet their mechanical weakness and potential burst release pose challenges for systemic administration.[13] Polymer micelles, while offering advantages such as enhanced drug solubility, targeted delivery, and prolonged circulation, still face challenges regarding their stability under physiological conditions and concerns about premature drug leakage.[14] In contrast, polydopamine (PDA) nanoparticles, a biomimetic nanomaterial, not only possess a high surface area for effective drug adsorption and loading but also exhibit diverse cellular uptake mechanisms, multi-drug responsive release characteristics, and good biocompatibility, making PDA nanoparticles widely applicable in the field of nanomedicine.[15] However, using PDA nanoparticles alone to deliver Danu lacks specificity. To address this limitation, this study proposes modifying PDA with boron phenylalanine (BPA) groups to enhance its targeting in NSCLC. Studies have shown that sialic acid is overexpressed on the surface of lung cancer cells,[16] and phenylalanine residues exhibit high affinity and selectivity for sialic acid,[17] providing a potential binding site for BPA-modified nanocarriers, thereby enabling preferential accumulation of the nanoparticles in tumor regions. Introducing BPA into the nanocarrier can enhance the transport of drug-loaded nanoparticles to tumors through sialic acid recognition, significantly improving drug accumulation and penetration at tumor sites, thereby enhancing the bioavailability of the drug in the body.[16]

Based on this, the present study utilized BPA-modified PDA as a carrier to load Danu, resulting in the preparation of B-PDA@Danu nanoparticles. This research combines the targeting of Aurora-A by Danu with the tumor-targeting capabilities of B-PDA nanoparticles, thereby achieving precise targeted therapy for NSCLC.

Materials and Methods

Preparation of B-PDA

Dopamine and benzoic acid mixture were stirred in a water solution with a pH of 10.0 for 12 hours to prepare nanoparticles with a dopamine to BPA mass ratio of 4:1. Subsequently, the nanoparticles were separated by centrifugation at a speed of 10,000 rpm for 10 minutes. The nanoparticles were then washed three times with deionized water using high-speed centrifugation at 10,000 rpm for 10 minutes, resulting in the final product, B-PDA.[17]

Preparation of B-PDA@Danu

B-PDA nanoparticles were suspended in water, and Danu (at a mass ratio of 1:10 to B-PDA) was added to the reaction solution, labeled as M1. The solution was then stirred for 12 hours, followed by centrifugation at 10,000 rpm for 10 minutes to separate and purify the product, which underwent three washes with deionized water. The concentration of free Danu in the supernatant after centrifugation (denoted as W1) was detected using HPLC, and the encapsulation efficiency was calculated using the formula:

$$\text{Encapsulation Efficiency} = (\text{M1} - \text{W1})/\text{M1} * 100\%$$

$$\text{Drug Loading} = (\text{M1} - \text{W1})/\text{M} * 100\%$$

Here, M represents the total mass of B-PDA@Danu.[18]

The synthesized B-PDA was identified using infrared spectroscopy. The microscopic morphology of B-PDA and B-PDA was observed using transmission electron microscopy. The particle size of B-PDA and B-PDA was measured using dynamic light scattering (DLS). The Zeta potential of B-PDA and B-PDA was determined using a nanoparticle size analyzer.

Extravasated Release Curve

Phosphate-buffered saline solution (PBS) containing 0.5% Tween 80 was utilized as the release medium to measure the release of Danu from B-PDA@Danu. B-PDA@Danu nanoparticles and Danu solution were loaded into a dialysis bag,

which was then placed in 20 mL of the release medium. The temperature of the shaker was set to 37°C with a shaking frequency of 100 rpm. At 1, 2, 4, 8, 12, 24, 36, and 48 hours, 1 mL of the release medium was withdrawn, and an equal volume of fresh release medium was added to maintain sink conditions. The content of Danu in each sample was determined using the HPLC method, and the cumulative release amount was calculated using the following formula:

$$S\% = \frac{\sum_{i=1}^{n-1} V_a C_i + V_0 C_n}{M} \times 100\%$$

Here, V_0 represents the total volume of the release medium (V_0 = 20 mL), V_a is the volume of the sample taken (V_a = 1 mL), C_n is the concentration of Danu at the nth sampling time, and M is the total amount of Danu.[19,20]

Cell Culture

The human normal lung epithelial cell line BEAS-2B (iCell-h023, iCell) and the human NSCLC cell line A549 (iCell-h011, iCell) were cultured in BEAS-2B cell-specific culture medium (iCell-h023-001b, iCell) and A549 cell-specific culture medium (iCell-h011-001b, iCell), respectively. All cells were maintained in a 5% CO_2 and 37°C CO_2 incubator.

Cell Counting Kit-8 (CCK8)

BEAS-2B and A549 cells were seeded in 96-well plates and cultured overnight. When the cell density reached approximately 75%, drug treatment was initiated. After 24 hours, the plates were removed from the incubator, old medium was aspirated, and fresh medium containing 10% CCK-8 was added. The plates were then further incubated at 37°C for 1.5 hours before being placed in a microplate reader, with absorbance measured at a wavelength of 450 nm.

① Different concentrations (0, 10, 20, 40, 80, 160, and 320 μg/mL) of B-PDA were used to treat BEAS-2B or A549 cells for 24 hours.

② A549 cells were treated with B-PDA, Danu, or B-PDA@Danu for 24 hours, with a constant Danu concentration of 1 μM. The quantity of B-PDA and B-PDA@Danu was calculated based on the drug loading of the microspheres (subsequent in vitro experiments involving drug treatment would follow the same protocol).

Cell Calcein AM/PI Straining

A549 cells were seeded in 6-well plates containing round coverslips and left overnight for cell adhesion and growth. Once the cell density reached approximately 80%, drug treatment was administered. After 24 hours, the culture was terminated. Cells were gently washed with PBS to remove any drug-containing medium that could interfere with the detection. Subsequently, 1 mL of Calcein AM/PI detection working solution was added to each well, and the cells were incubated at 37°C in the dark for 30 minutes. After the incubation period, the coverslips were removed, mounted on glass slides, and observed under a fluorescence microscope to assess cell staining.[21]

Cell Uptake

Cyanine5 (Cy5) fluorescent dye (DuoFluor) was used in place of Danu to prepare B-PDA@CY5. The uptake behavior of A549 cells towards B-PDA@CY5 was studied at 1, 2, and 4 hours using a fluorescence microscope.[22]

Western Blot

Total protein was extracted from A549 cells or tumor tissue using RIPA lysis buffer. Following protein concentration determination, quantification, and denaturation by boiling, the proteins were loaded onto a polyacrylamide gel for electrophoresis. Once the target proteins were visibly separated, the electrophoresis was stopped, and the target proteins were transferred from the gel to a polyvinylidene fluoride (PVDF) membrane. The PVDF membrane was then immersed in a blocking solution and incubated for 1 hour. Specific primary antibodies were added and allowed to incubate overnight at 4°C. The next day, corresponding secondary antibodies were added (incubated for 1 hour) to bind to the primary antibodies on the membrane. Unbound secondary antibodies were washed away, and an enzyme substrate was added onto the membrane. The membrane was placed in a chemiluminescence imager for visualization. Antibodies used:

Cyclin B1 (ab181593, Abcam), Bax (ab32503, Abcam), GAPDH (ab8245, Abcam), p53 (10,442-1-AP, Proteintech), Bcl-2 (26,593-1-AP, Proteintech), GAPDH (60004-1-Ig, Proteintech), γ-H2A.X (ab81299, Abcam).

Cell Cycle Analysis

After drug treatment, A549 cells were collected and the cell density was adjusted to 1×10^6 cells/mL. A 1 mL single-cell suspension was taken, centrifuged at 1000 rpm for 3 minutes, and the supernatant was removed. Subsequently, 500 μL of 70% cold ethanol was added to the cells for fixation. After fixation, 500 μL of pre-prepared PI/RNaseA staining solution (F10797, ThermoFisher) was added to the cells, and they were incubated at room temperature in the dark for 30–60 minutes. Finally, fluorescence at the excitation wavelength of 488 nm was recorded using a flow cytometer.

Construction of Subcutaneous Tumor Xenografts in Mice

Fifty-one male BALB/c-nu nude mice (5 weeks old, weighing 17–20 g) were purchased from Sibeifu (Beijing) Biotechnology Co., Ltd.

Twenty mice were randomly selected and subcutaneously injected with 100 μL of A549 cell suspension at a density of 1×10^6 cells/mL to establish subcutaneous tumor xenograft models. The successful establishment of the xenograft model was confirmed when the tumor volume reached 100 mm^3.

The mice were then randomly divided into Saline group, B-PDA group, Danu group, and B-PDA@Danu group, with 5 mice in each group. In the Danu group, mice were treated with 30 mg/kg Danu via tail vein injection. The B-PDA group and B-PDA@Danu group received B-PDA and B-PDA@Danu treatments via tail vein injection, respectively (Calculate the corresponding doses of B-PDA and B-PDA@Danu based on a loading dose of 30 mg/kg Danu). The Saline group received an equivalent volume of saline via tail vein injection as a control. Dosage administration occurred every 2 days with weight measurements, and the treatment concluded after 14 days.

Hematoxylin and Eosin (HE) Staining

Tissues, following steps such as fixation in paraformaldehyde, dehydration in xylene and ethanol, embedding in paraffin, and sectioning with a microtome, were prepared into 4 μm-thin sections and mounted on glass slides. The tissues were stained using the standard HE staining protocol. Subsequently, the slides were sealed with neutral resin, air-dried, and then observed and captured under an optical microscope.

Hemolytic Analysis

Fresh mouse blood (1 mL) was added to a centrifuge tube containing 10 mL of PBS, centrifuged, the supernatant discarded, and the precipitated red blood cells washed using the same method. This washing process was repeated 2–3 times until the supernatant no longer showed a red color. The collected blood cells were then added to 10 mL of PBS to create a cell suspension.

Subsequently, 200 μL of the blood cell suspension was added to separate Eppendorf tubes containing 800 μL of different concentrations (50, 100, 200, 300, and 400 μg/mL) of B-PDA@Danu, 800 μL of PBS (negative control), and 800 μL of Triton X-100 (positive control). The Eppendorf tubes were placed in a centrifuge set at 3000 rpm and 4°C for 5 minutes. After centrifugation, images were captured, and the Optical Density (OD) was measured at 570 nm to calculate the hemolysis rate. The experiment was independently repeated three times.

Blood and Biochemical Index Analysis

Fresh blood samples were collected from the mouse eye socket, left to stand at room temperature for 30 minutes, then centrifuged at 1000 rpm/min for 15 minutes at 4°C. The supernatant was collected for analyzing blood and biochemical markers related to the liver, kidney, and heart (Red blood cell (RBC), White blood cell (WBC), Platelet (PLT), Hemoglobin (HGB), glutamic pyruvic transaminase (ALT), glutamic oxaloacetic transaminase (AST), creatine kinase (CK), lactate dehydrogenase (LDH)).

Construction of Mouse Lung Orthotopic Tumor Model

Using the remaining 31 male BALB/c nude mice, a mouse A549 lung orthotopic tumor model was constructed. The mice were anesthetized, and the chest wall was disinfected with 70% alcohol. A 5–7 mm skin incision was made below the scapula of the chest, along the mid-axillary line dorsally (approximately 1.5 cm above the lower rib line). While monitoring lung movements, a 40 μL PBS mixture containing 1×10^6 A549 cells was slowly injected into the lung parenchyma, and the incision was sutured. The mice in the Sham group underwent the same procedure but were injected with PBS solution without cells.[23]

Twenty-five A549 lung orthotopic tumor model mice were divided into 5 groups: Sham group, Saline group, B-PDA group, Danu group, and B-PDA@Danu group, each consisting of 5 mice. After 2 weeks of inoculation, the mice were treated with B-PDA, Danu, or B-PDA@Danu via tail vein injection (each group equivalent to 30 mg/kg Danu).[8] The control group received injections of the corresponding volume of saline as a control. Dosage administration occurred every 2 days with weight measurements, and the treatment concluded after 14 days.

Data Statistics and Analysis

Collect data from at least three independent replicates. Utilize GraphPad Prism 8.0 for statistical analysis and plotting. Data will be presented as mean ± standard deviation. Between-group comparisons will be conducted using one-way analysis of variance, while changes in tumor volume or mouse weight over time will be analyzed using two-way analysis of variance. Differences will be considered statistically significant when the P-value is less than 0.05.

Results

Characterization of B-PDA and B-PDA@Danu

From the infrared spectrum in Figure 1A, compared to PDA, the infrared spectrum of B-PDA not only exhibited the characteristic stretching vibration peaks of PDA (–OH, $–NH_2$, –C=C–, –C=N, and C–N–C groups), but also displayed a stretching vibration peak of B–N near 1380 cm^{-1}, indicating the successful synthesis of B-PDA. Results in Figure 1B–E showed that the synthesized B-PDA is spherical with an average particle size of (154.79±4.29) nm and an average potential of −25.8±1.11. After loading Danu, the shape remained unchanged, with a slightly increased average particle size of (172.96±1.61) nm and an elevated Zeta average potential of −31.5±0.41 (Figure 1B–E). The measurement of the hydrated particle size within 7 days can reflect the stability of nanospheres. Figure 1F demonstrated that there is no significant difference in particle size of B-PDA and B-PDA@Danu over 7 days, indicating good stability of both formulations. The in vitro release behavior of Danu was shown in Figure 1G, revealing that free Danu rapidly releases in the release medium, with a high cumulative release rate of (90.23±1.58) % at 12 hours. In contrast, the cumulative release rate of B-PDA@Danu was only (73.87±4.15) % at 24 hours and reached (82.98±2.45) % at 48 hours, confirming the sustained release effect of B-PDA and B-PDA@Danu. Additionally, the encapsulation efficiency of Danu was measured to be (90.50±2.31) %, with a drug loading capacity of (8.30±0.19) %.

Impact of B-PDA@Danu on NSCLC Cells

To evaluate the cytotoxicity of the biomaterial, unloaded B-PDA was applied to human normal lung epithelial cell line BEAS-2B and human NSCLC cell line A549. Results in Figure 2A and B demonstrated that even at a high concentration (320 μg/mL) of B-PDA, there was no significant decrease in the viability of BEAS-2B and A549 cells, indicating low cytotoxicity of B-PDA.

Furthermore, we assessed the impact of B-PDA@Danu on NSCLC cells. The CCK8 results in Figure 2C showed a significant decrease in cell viability for both the B-PDA and B-PDA@Danu groups of A549 cells, with the inhibitory effect of B-PDA on A549 cell viability being significantly stronger than that of free Danu. The cell AM/PI staining experiment (Figure 2D) revealed the highest amount of red fluorescence in the B-PDA@Danu group, indicating the highest cell death, consistent with the CCK8 results, further demonstrating the superior anti-tumor effect of B-PDA@Danu over free B-PDA.

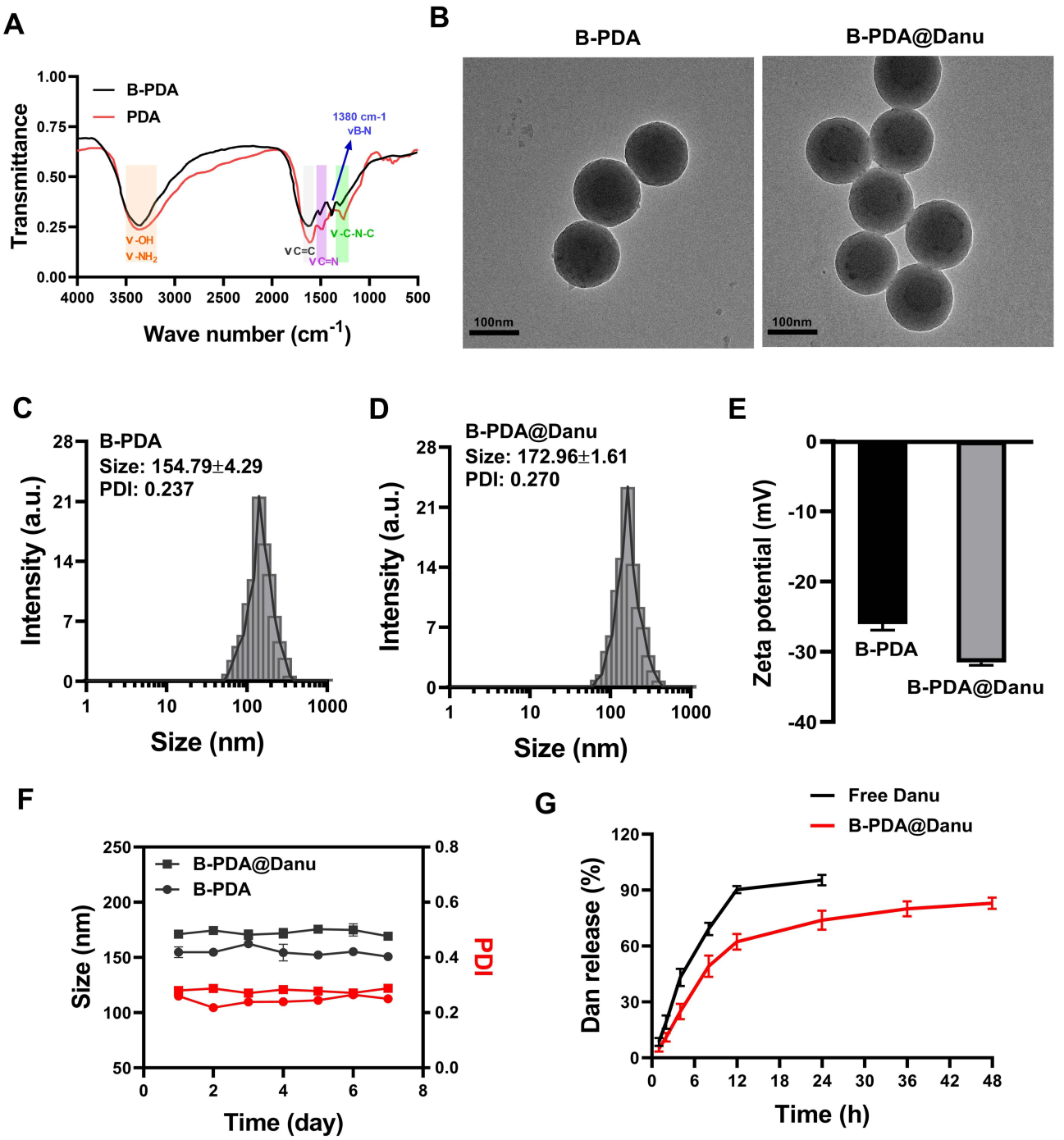

Figure 1 Characterization of B-PDA and B-PDA@Danu. (**A**) FT-IR spectrum of PDA and B-PDA. (**B**) TEM images of B-PDA and B-PDA@Danu. (**C**) Particle size distribution of B-PDA. (**D**) Particle size distribution of B-PDA@Danu. (**E**) Zeta potential of B-PDA and B-PDA@Danu. (**F**) Hydrated particle size of B-PDA and B-PDA@Danu over 7 days. (**G**) In vitro release curves of free Danu and B-PDA@Danu.

In this study, CY5 fluorescent dye was used instead of Danu to observe the impact of B-PDA on cell uptake. As shown in Figure 2E, A549 cells exhibited limited uptake of free CY5, but after encapsulation in B-PDA, the cellular uptake significantly increased, indicating that B-PDA facilitates cellular uptake of the drug.

Further analysis of apoptotic levels in each group was performed using flow cytometry (Figure 3A). The results demonstrated that both free Danu and B-PDA@Danu significantly increased the apoptosis rate of A549 cells ($P < 0.001$). Notably, B-PDA@Danu exhibited a markedly stronger pro-apoptotic effect compared to free Danu ($P < 0.001$).

https://doi.org/10.2147/IJN.S519608

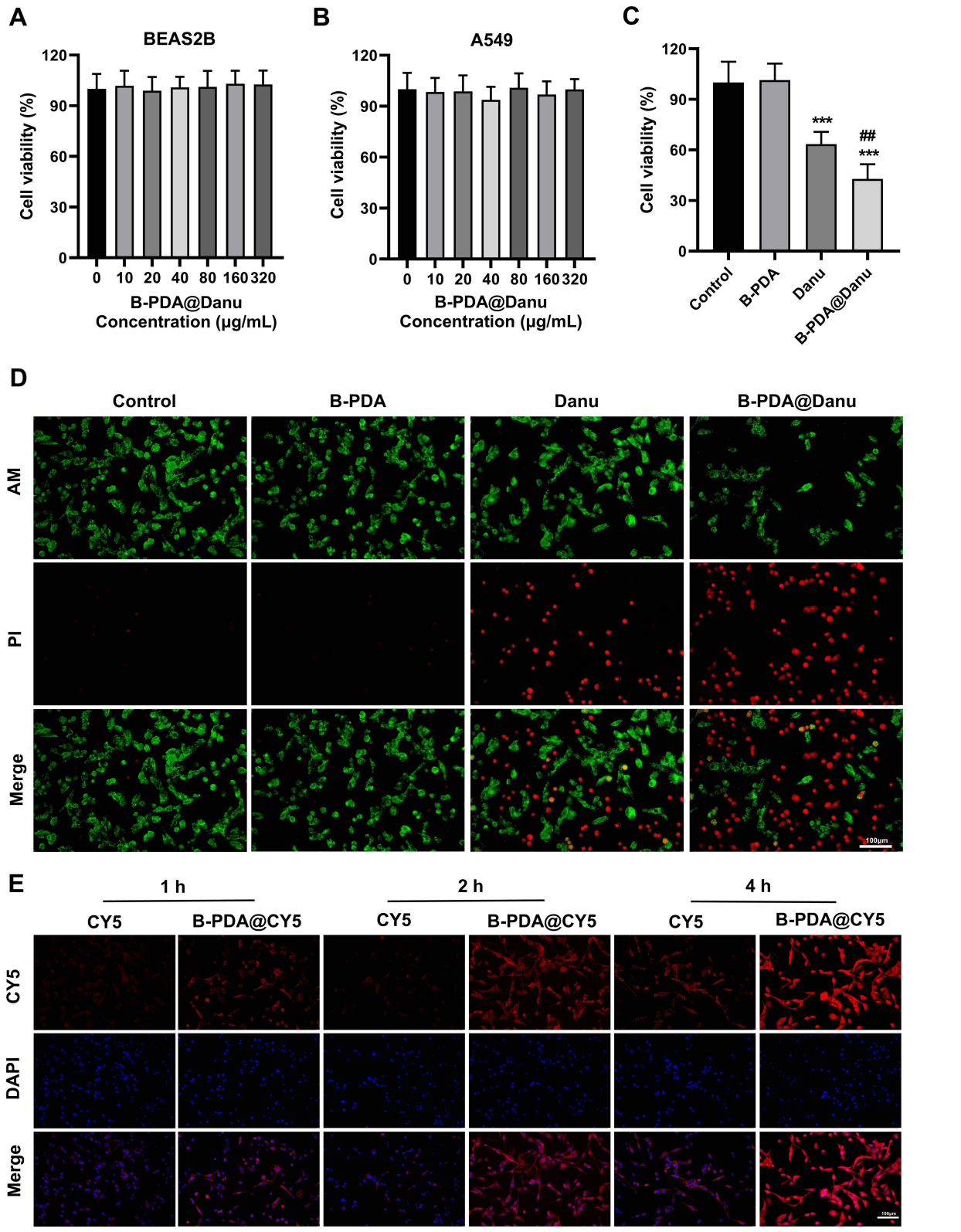

Figure 2 Impact of B-PDA@Danu on A549 cell viability, apoptosis, and uptake. (**A**) Viability of BEAS-2B cells after 24-hour exposure to different concentrations (0, 10, 20, 40, 80, 160, and 320 μg/mL) of B-PDA. (**B**) Viability of A549 cells after 24-hour exposure to different concentrations (0, 10, 20, 40, 80, 160, and 320 μg/mL) of B-PDA. (**C**) Viability of A549 cells after 24-hour exposure to different treatments. (**D**) Apoptosis of A549 cells after 24-hour exposure to different treatments. (**E**) Uptake of free CY5 and B-PDA@CY5 by cells. ***P < 0.001 vs Control, ##P < 0.01 vs Danu.

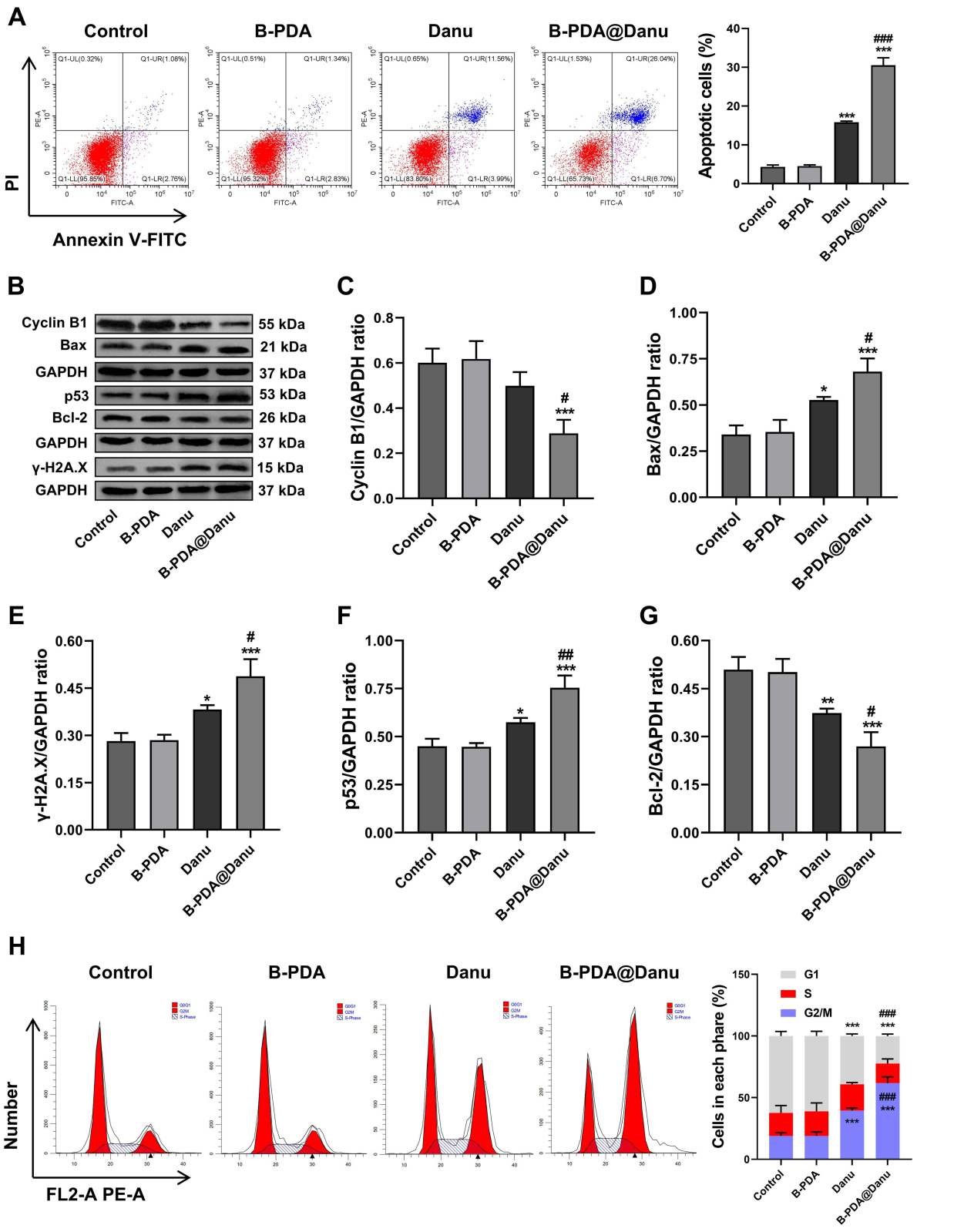

Figure 3 Impact of B-PDA@Danu on the cell cycle of A549 cells. (**A**) Representative flow cytometry plots of cell apoptosis and corresponding quantitative analysis. (**B**–**G**) Relative expression levels and quantitative analysis of apoptosis-related proteins, cell cycle-related proteins, and DNA damage-related proteins in each group. (**H**) Representative flow cytometry plots of cell cycle distribution and corresponding quantitative analysis. *P < 0.05, **P < 0.01 and ***P < 0.001 vs Control, $^{\#}$P < 0.05, $^{\#\#}$P < 0.01 and $^{\#\#\#}$P < 0.001 vs Danu.

https://doi.org/10.2147/IJN.S519608

As depicted in Figure 3B–G, Western blot analysis revealed that the B-PDA@Danu group exhibited significant upregulation of the pro-apoptotic protein Bax and downregulation of the anti-apoptotic protein Bcl2 expression compared to other groups, once again confirming the excellent anti-tumor effect of B-PDA@Danu. Moreover, after co-incubation of B-PDA@Danu with A549 cells for 24 hours, B-PDA@Danu induced a notable elevation in DNA damage markers, including p53 and γ-H2A.X proteins, suggesting its ability to trigger DNA damage. Concurrently, the significant downregulation of G2/M phase-related protein cyclin B1 expression indicated a possible cell cycle arrest at the G2 phase, thereby inhibiting cell proliferation. Consistently, the flow cytometry analysis in Figure 3H demonstrated that B-PDA@Danu can significantly induce cell cycle arrest at the G2/M phase, aligning with the Western blot findings.

Impact of B-PDA@Danu on Subcutaneous Transplant Tumors in Mice

To investigate the in vivo anti-tumor effects of B-PDA@Danu, we established a subcutaneous xenograft tumor model and treated groups of mice with B-PDA, Danu, or B-PDA@Danu. Throughout the treatment period, the body weights of the mice in each group remained stable without significant changes (Figure 4A). However, compared to the Sal group mice, tumor growth significantly slowed down in mice treated with Danu or B-PDA@Danu (Figure 4B and C). Notably, the inhibitory effect of B-PDA@Danu on tumor growth was markedly stronger than that of Danu (Figure 4B and C). Consistent with our expectations, mice in the B-PDA@Danu group exhibited evident pathological damage in tumor tissues, characterized by severe nuclear dissolution and shrinkage of tumor cells, indicating substantial damage to the tumor tissue (Figure 4D). Subsequently, we further investigated the effects of B-PDA@Danu on apoptosis, cell cycle, and the expression of DNA damage-related proteins in vivo. As shown in Figure 4E–J, following treatment with B-PDA@Danu, the expression of Bax, p53, and γ-H2A.X was significantly upregulated, while the expression of Bcl2 and cyclin B1 was significantly downregulated. These findings suggest that B-PDA@Danu may induce DNA damage, affect the cell cycle, and ultimately lead to tumor cell apoptosis. These results collectively demonstrate that B-PDA@Danu can significantly inhibit tumor growth without causing weight loss in mice. Its mechanism of action may involve cell cycle arrest, DNA damage, and apoptotic pathways, highlighting the tremendous potential of B-PDA@Danu in the treatment of NSCLC.

Safety Evaluation of B-PDA@Danu

To further assess the safety of B-PDA@Danu for in vivo applications, we evaluated its blood compatibility and its effects on major organs and tissues in mice. The results in Figure 5A and B demonstrate that at various concentration gradients (0, 50, 100, 200, 400, and 800 μg/mL), the hemolysis rate of B-PDA@Danu was less than 3%, indicating good blood compatibility. HE staining results of the heart, liver, spleen, and kidneys in the Sal group and B-PDA@Danu group showed well-arranged cells with homogeneous cytoplasm, and normal histopathological evaluations (Figure 5C). Additionally, there were no significant differences in blood, liver, kidney, and cardiac-related parameters (RBC, WBC, PLT, HGB, ALT, AST, CK, and LDH) between the B-PDA@Danu group and the Sal group, indicating low blood, liver, kidney, and cardiac toxicity of B-PDA@Danu (Figure 5D–K). These data collectively demonstrate that B-PDA@Danu exhibits good biocompatibility and safety.

Distribution of B-PDA@Danu in Mice

To investigate whether B-PDA@Danu can effectively target and accumulate at the site of carcinogenesis, we established a mouse lung in situ cancer model and used IR780 fluorescent dye instead of Danu to study the in vivo distribution of the drug after intravenous administration (Figure 6A). Live imaging of mice revealed that at 24 hours, the pulmonary fluorescence in the IR780 group was very weak, while the B-PDA@IR780 group still exhibited a strong fluorescence signal, indicating the strong tumor site retention effect of B-PDA@IR780 (Figure 6B). Mice were dissected at 24 hours post-injection, and heart, liver, spleen, lung, and kidney tissues were collected to observe the distribution of IR780 in each tissue. The results showed that at 24 hours, the lung tissue in the B-PDA@IR780 group still exhibited a strong fluorescence signal (Figure 6C).

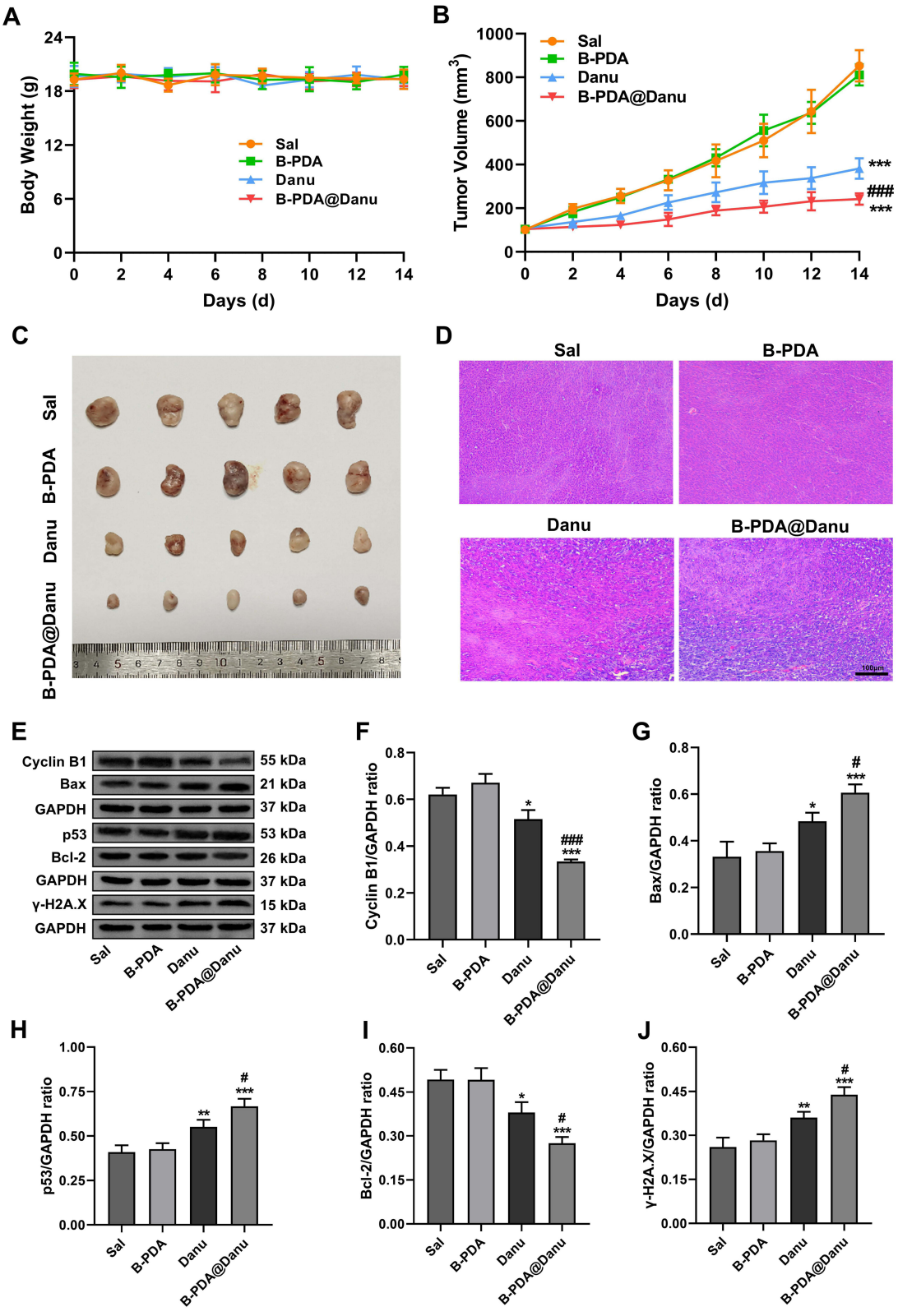

Figure 4 Effects of B-PDA@Danu on subcutaneous xenograft tumors in mice. (**A**) Mouse body weight changes. (**B** and **C**) Changes in tumor volume in mice. (**D**) Mouse tumor HE staining. (**E–J**) Relative expression levels and quantitative analysis of apoptosis-related proteins, cell cycle-related proteins, and DNA damage-related proteins in mouse tumor tissues. *P < 0.05, **P < 0.01 and ***P < 0.001 vs Control, $^{\#}$P < 0.05 and $^{\#\#\#}$P < 0.001 vs Danu.

https://doi.org/10.2147/IJN.S519608

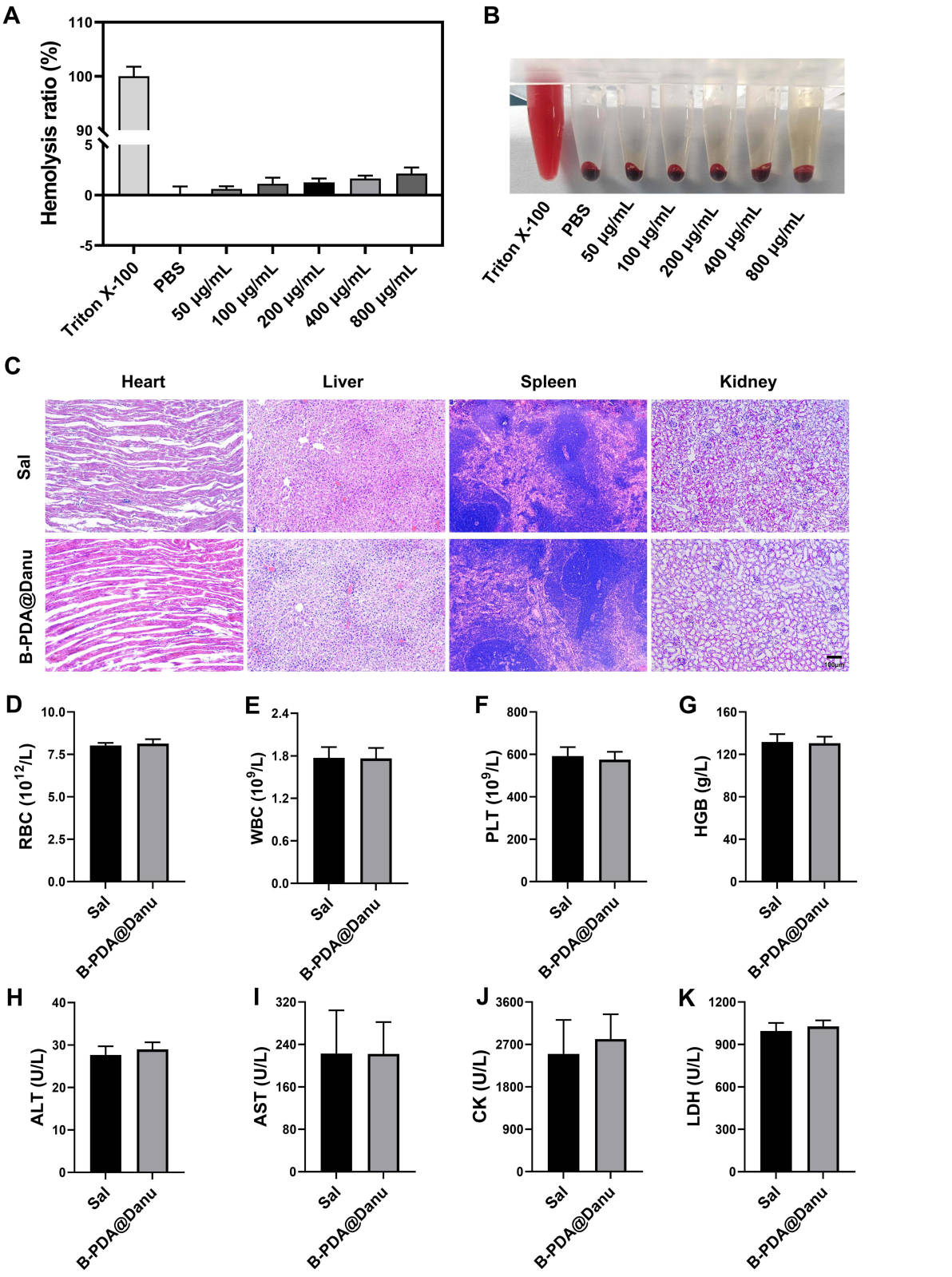

Figure 5 Safety Evaluation of B-PDA@Danu. (**A** and **B**) Hemolysis analysis. (**C**) HE staining of mouse heart, liver, spleen, and kidneys. (**D**–**K**) Relative levels of serum RBC, WBC, PLT, HGB, ALT, AST, CK, and LDH in each group of mice.

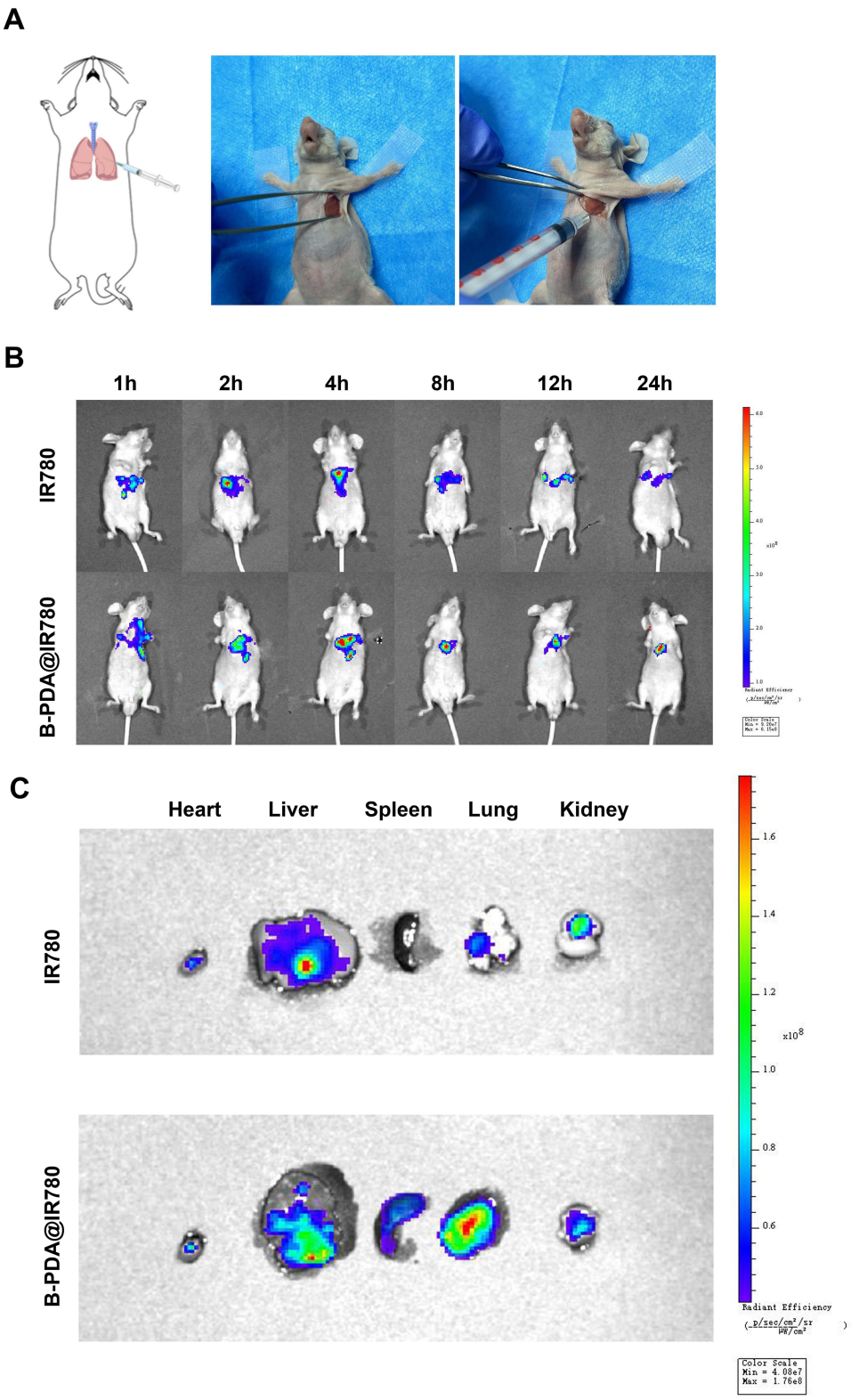

Figure 6 Distribution of B-PDA@Danu in vivo. (**A**) Schematic diagram and representative images of the lung in situ tumor model. (**B**) In vivo imaging of mice at 1, 2, 4, 8, 12, and 24 hours post-dosing. (**C**) Tissue distribution imaging at 24 hours post-dosing.

https://doi.org/10.2147/IJN.S519608

Effects of B-PDA@Danu on Mouse Lung in Situ Transplant Tumors

In the mouse lung cancer in situ model, we further investigated the effects of B-PDA@Danu on NSCLC. During the treatment period, mice in the Sal and B-PDA groups showed a decreasing trend in body weight and poor overall condition, while mice in the Danu group maintained relatively stable body weight initially but started to decrease later on. In contrast, mice in the B-PDA@Danu group maintained relatively stable body weight throughout the treatment (Figure 7A). After the treatment concluded, the lung tissues of mice in each group were weighed. The lung weight of the B-PDA@Danu group was significantly lower than that of the Sal group, with no significant difference compared to the Sham group (Figure 7B). This to some extent may reflect a decrease in tumor density in the lung tissues of mice in the B-PDA@Danu group. Histological examination of lung tissues using HE staining revealed that after treatment with

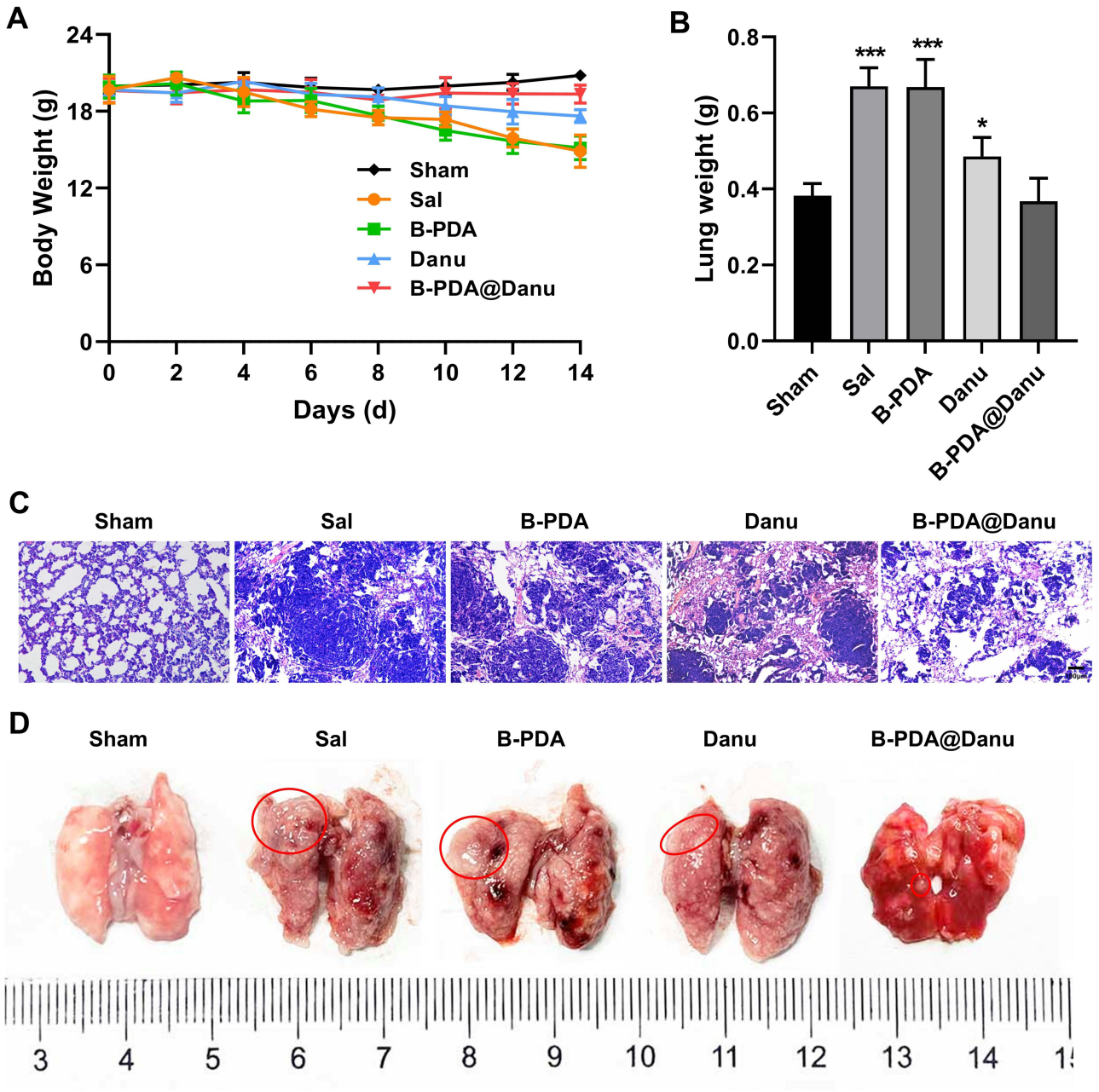

Figure 7 The effects of B-PDA@Danu on mouse lung orthotopic transplantation tumors. (**A**) Changes in body weight of mice during treatment. (**B**) Lung tissue weights of mice in each group. (**C**) HE staining of lung tissues from mice in each group (100× magnification). (**D**) External appearance of lung tissues (The red circle marks the tumor). *P < 0.05 and ***P < 0.001 vs Sham.

 https://doi.org/10.2147/IJN.S519608

B-PDA@Danu, the area occupied by tumors in the lung tissues (dark regions) decreased (Figure 7C). Following the treatment, the appearance of lung tissues is shown in Figure 7D. Both the Sal and B-PDA groups exhibited large tumor masses in the lung tissues, while the lung tumors in the Danu and B-PDA@Danu groups showed varying degrees of shrinkage, with the tumors in the B-PDA@Danu group demonstrating the most significant size reduction.

Discussion

The research application of nanotechnology in the medical field provides NSCLC patients with the opportunity to receive more effective treatments. Nanoparticles, not only as a special form of nanomaterial, dominate the field of nanomedicine applications, but also represent a current research hotspot in NSCLC therapy. The Aurora-A inhibitor Danu has shown significant potential in previous studies for its anti-tumor effects. However, due to issues such as targeting efficiency, its clinical application remains limited.[8,24,25] Therefore, in this study, B-PDA@Danu nanoparticles with a precise targeting effect were prepared for delivering Danu. These nanoparticles can effectively target and accumulate at the tumor site, leading to tumor shrinkage.

Over the past two decades, due to its strong ability to enter different cell types, the convenience of surface modification with other biomolecules, and good biocompatibility, PDA has been used as a classic drug-loaded nanoparticle for drug delivery to disease sites.[15,26–28] Additionally, PDA has a high surface area, which allows for effective drug adsorption and encapsulation. In this study, the encapsulation efficiency of the synthesized B-PDA@Danu nanoparticles was (90.50±2.31) %, with a drug loading capacity of (8.30±0.19) %. However, using PDA alone as a carrier cannot avoid the non-selective distribution of drugs, leading to systemic toxicity. Sialic acid is overexpressed on the cell membrane of tumor cells and is associated with metastasis, progression, and resistance to chemotherapy, serving as a tumor marker.[18,29] Recent studies have shown that BPA can specifically interact with sialic acid residues on the surface of cancer cells.[30] Introducing BPA into drug delivery systems can enhance drug accumulation and penetration at tumor sites, facilitating drug uptake by tumor cells.[31,32] Therefore, in this study, BPA was used to modify the surface of PDA, as evidenced by the characteristic δB-N infrared absorption band at 1380 cm−1, confirming the successful synthesis of B-PDA.

The surface charge of nanoparticles plays a pivotal role in cellular uptake and biodistribution. Our synthesized B-PDA@Danu exhibited a highly negative zeta potential of −31.5 ± 0.41 mV, which may significantly influence their biological behavior. Studies have suggested that moderate negative charges could enhance receptor-mediated endocytosis in cancer cells overexpressing sialic acid.[33] This aligns with our findings of significantly improved cellular uptake of B-PDA@Danu compared to free Danu. Furthermore, the negative surface charge may contribute to prolonged circulation time by minimizing opsonization and macrophage clearance, thereby enhancing tumor accumulation. More notably, this surface feature may facilitate cellular internalization via enhanced electrostatic interactions with positively charged domains of cancer cell membranes.[34] Previous research has shown that by encapsulating drugs using nanotechnology, it is possible to reduce the toxic side effects of drugs on other organs, improve the bioavailability of drugs in tumor cells, achieve drug sustained release, reduce dosing frequency and amount;[35,36] and increase drug retention time at tumor sites, enhancing drug uptake by tumor cells.[17] As demonstrated in our biosafety assays, the low hemolysis rate and the absence of histological toxicity in major organs suggest that the negative surface charge contributes not only to improved uptake but also to an excellent safety and immunogenicity profile in vivo. This electrostatic profile may be particularly advantageous in minimizing off-target effects and systemic toxicity, thus enhancing the therapeutic index of the nanomedicine.

Research has indicated that Aurora-A can promote tumorigenesis and development through various mechanisms, including facilitating cell cycle progression, activating cell survival signals, and anti-apoptotic pathways.[6,37,38] Aurora-A is found to be overexpressed in various cancers, including NSCLC, making it a potential target for cancer therapy.[5–7,39] A small molecule Aurora-A inhibitor, Danu, has been identified to exhibit significant inhibitory effects on the Aurora-A family and is being investigated in clinical trials as a promising candidate for cancer treatment.[8,40] In this study, Danu was shown to inhibit the viability of A549 cells in vitro, induce apoptosis in A549 cells, inhibit tumor growth in vivo, induce damage to tumor tissues, and lead to tumor shrinkage. The use of B-PDA for delivering Danu further enhanced its anti-tumor effects and demonstrated good biocompatibility.

More importantly, our findings revealed that B-PDA@Danu significantly induced G2/M phase cell cycle arrest in A549 cells. This arrest plays a pivotal role in anti-cancer therapy as it halts cells at a critical checkpoint before mitotic division, effectively blocking the proliferation of rapidly dividing tumor cells.[41] Prolonged arrest at this phase often triggers intrinsic apoptotic pathways, further reinforcing the cytotoxicity of the therapeutic agent. The suppression of Cyclin B1 expression observed in our study confirms the interruption of mitotic progression, while the concomitant upregulation of p53 and γ-H2A.X indicates substantial genotoxic stress. p53, a guardian of the genome, orchestrates DNA damage response and either promotes cell cycle arrest for repair or initiates apoptosis upon irreparable damage. The persistent upregulation of these markers upon B-PDA@Danu treatment not only reflects effective DNA damage but also suggests the potential for long-term therapeutic suppression of tumor recurrence. These results collectively demonstrate that B-PDA@Danu can significantly inhibit tumor growth without causing weight loss in mice, and that the mechanism of action may involve cell cycle arrest, DNA damage, and apoptotic pathways.

Conclusion

In this study, we developed a novel nano-drug delivery system, B-PDA@Danu, by employing BPA-modified PDA nanoparticles for the targeted delivery of the Danu in the treatment of NSCLC. The B-PDA@Danu nanoparticles exhibited high drug encapsulation efficiency and selective tumor-targeting ability. In vitro, B-PDA@Danu significantly enhanced cellular drug uptake, induced G2/M phase arrest, upregulated p53 and γ-H2A.X, and downregulated Cyclin B1, ultimately leading to apoptosis in A549 cells. In vivo, B-PDA@Danu demonstrated superior tumor accumulation, prolonged intratumoral drug retention, effective tumor growth inhibition, and favorable biocompatibility compared with free Danu. Collectively, these results highlight the potent therapeutic potential of B-PDA@Dan as a targeted and efficient delivery platform for NSCLC treatment.

Abbreviations

NSCLC, non-small cell lung cancer; Danu, Danusertib; PDA, Polydopamine; BPA, phenylboronic acid; PBS, Phosphate-buffered saline solution; CCK8, Cell Counting Kit-8; Cy5, Cyanine5; PVDF, polyvinylidene fluoride; HE, Hematoxylin and eosin; OD, Optical Density; RBC, Red blood cell; WBC, White blood cell; PLT, Platelet; HGB, Hemoglobin; ALT, glutamic pyruvic transaminase; AST, glutamic oxaloacetic transaminase; CK, creatine kinase; and LDH, lactate dehydrogenase.

Data Sharing Statement

Data will be made available from the corresponding author upon reasonable request.

Ethical Statement

The experiment was approved by the Wenzhou Medical University Experimental Animal Ethics Committee (wydw2024-0602).

Animal Rights

All animal research was conducted in accordance with the standards outlined in the 8th edition of "Guide for the Care and Use of Laboratory Animals" published by the National Academy of Sciences, National Academies Press, Washington, D.C.

Funding

This work was supported by Wenzhou Science and Technology Bureau Medical and Health Project (number Y20240019), Competitive Research Project of Quzhou Science & Technology Bureau (2023k114), and National Clinical Key Specialty Internal Fund of Quzhou Hospital Affiliated of Wenzhou Medical University (Internal Research Project) (GJZK-02).

Disclosure

The authors report no conflicts of interest in this work.

References

1. Sung H, Ferlay J, Siegel RL, et al. Global cancer statistics 2020: GLOBOCAN estimates of incidence and mortality worldwide for 36 cancers in 185 countries. *CA Cancer J Clin*. 2021;71(3):209–249. doi:10.3322/caac.21660
2. Yu H, Li SB. Role of LINC00152 in non-small cell lung cancer. *J Zhejiang Univ Sci B*. 2020;21(3):179–191. doi:10.1631/jzus.B1900312
3. Mithoowani H, Febbraro M. Non-small-cell lung cancer in 2022: a review for general practitioners in oncology. *Curr Oncol*. 2022;29 (3):1828–1839. doi:10.3390/curroncol29030150
4. Barr AR, Gergely F. Aurora-A: the maker and breaker of spindle Poles. *J Cell Sci*. 2007;120(Pt 17):2987–2996. doi:10.1242/jcs.013136
5. Zi D, Zhou ZW, Yang YJ, et al. Danusertib induces apoptosis, cell cycle arrest, and autophagy but inhibits epithelial to mesenchymal transition involving PI3K/Akt/mTOR signaling pathway in human ovarian cancer Cells. *Int J Mol Sci*. 2015;16(11):27228–27251. doi:10.3390/ijms161126018
6. Yan M, Wang C, He B, et al. Aurora-A kinase: a potent oncogene and target for cancer therapy. *Med Res Rev*. 2016;36(6):1036–1079. doi:10.1002/med.21399
7. Zheng X, Chi J, Zhi J, et al. Aurora-A-mediated phosphorylation of LKB1 compromises LKB1/AMPK signaling axis to facilitate NSCLC growth and migration. *Oncogene*. 2018;37(4):502–511. doi:10.1038/onc.2017.354
8. Zhang X, Lei Y, Chen X, et al. Suppression of NSCLC progression via the co-administration of Danusertib, an AURK inhibitor, and KRIBB11, an HSF1 inhibitor. *Biochem Pharmacol*. 2024;223:116155. doi:10.1016/j.bcp.2024.116155
9. Carpinelli P, Ceruti R, Giorgini ML, et al. PHA-739358, a potent inhibitor of aurora kinases with a selective target inhibition profile relevant to cancer. *Mol Cancer Ther*. 2007;6(12 Pt 1):3158–3168. doi:10.1158/1535-7163.MCT-07-0444
10. Khan KU, Minhas MU, Badshah SF, Suhail M, Ahmad A, Ijaz S. Overview of nanoparticulate strategies for solubility enhancement of poorly soluble drugs. *Life Sci*. 2022;291:120301. doi:10.1016/j.lfs.2022.120301
11. Peng S, Xiao F, Chen M, Gao H. Tumor-microenvironment-responsive nanomedicine for enhanced cancer immunotherapy. *Adv Sci*. 2022;9(1): e2103836. doi:10.1002/advs.202103836
12. Dymek M, Sikora E. Liposomes as biocompatible and smart delivery systems–the current state. *Adv Colloid Interface Sci*. 2022;309:102757. doi:10.1016/j.cis.2022.102757
13. Jacob S, Nair AB, Shah J, Sreeharsha N, Gupta S, Shinu P. Emerging role of hydrogels in drug delivery systems, tissue engineering and wound management. *Pharmaceutics*. 2021;13(3):357. doi:10.3390/pharmaceutics13030357
14. Kotta S, Aldawsari HM, Badr-Eldin SM, Nair AB, Yt K. Progress in polymeric micelles for drug delivery applications. *Pharmaceutics*. 2022;14 (8):1636. doi:10.3390/pharmaceutics14081636
15. Liang Z, He Y, Ieong CS, Choi CHJ. Cell-nano interactions of polydopamine nanoparticles. *Curr Opin Biotechnol*. 2023;84:103013. doi:10.1016/j.copbio.2023.103013
16. Elgohary MM, Helmy MW, Abdelfattah EA, et al. Targeting sialic acid residues on lung cancer cells by inhalable boronic acid-decorated albumin nanocomposites for combined chemo/herbal therapy. *J Control Release*. 2018;285:230–243. doi:10.1016/j.jconrel.2018.07.014
17. Dai L, Liu J, Zhao X, et al. BPA-containing polydopamine nanoparticles for boron neutron capture therapy in a u87 glioma orthotopic model. *Adv Funct. Mater*. 2023;33(23):2214145. doi:10.1002/adfm.202214145
18. Yang F, Dai L, Shi K, et al. A facile boronophenylalanine modified polydopamine dual drug-loaded nanoparticles for enhanced anti-tumor immune response in hepatocellular carcinoma comprehensive treatment. *Biomaterials*. 2024;305:122435. doi:10.1016/j.biomaterials.2023.122435
19. Li W, Chen L, Gu Z, et al. Co-delivery of microRNA-150 and quercetin by lipid nanoparticles (LNPs) for the targeted treatment of age-related macular degeneration (AMD). *J Control Release*. 2023;355:358–370. doi:10.1016/j.jconrel.2023.01.080
20. Jaradat E, Weaver E, Meziane A, Lamprou DA. Microfluidic paclitaxel-loaded lipid nanoparticle formulations for chemotherapy. *Int J Pharm*. 2022;628:122320. doi:10.1016/j.ijpharm.2022.122320
21. Wang S, Xiong Y, Lalevée J, Xiao P, Liu J, Xing F. Biocompatibility and cytotoxicity of novel photoinitiator π-conjugated dithienophosphole derivatives and their triggered polymers. *Toxicol in vitro*. 2020;63:104720. doi:10.1016/j.tiv.2019.104720
22. Huang S, Xu Z, Zhi W, et al. pH/GSH dual-responsive nanoparticle for auto-amplified tumor therapy of breast cancer. *J Nanobiotechnology*. 2024;22(1):324. doi:10.1186/s12951-024-02588-0
23. Yue C, Zhang C, Alfranca G, et al. Near-infrared light triggered ROS-activated theranostic platform based on Ce6-CPT-UCNPs for simultaneous fluorescence imaging and chemo-photodynamic combined therapy. *Theranostics*. 2016;6(4):456–469. doi:10.7150/thno.14101
24. Shang YY, Yu N, Xia L, et al. Augmentation of danusertib's anticancer activity against melanoma by blockage of autophagy. *Drug Deliv Transl Res*. 2020;10(1):136–145. doi:10.1007/s13346-019-00668-5
25. Li S, Xu S, Liang X, et al. Nanotechnology: breaking the current treatment limits of lung cancer. *Adv Healthc Mater*. 2021;10(12):e2100078. doi:10.1002/adhm.202100078
26. Wang Z, Duan Y, Duan Y. Application of polydopamine in tumor targeted drug delivery system and its drug release behavior. *J Control Release*. 2018;290:56–74. doi:10.1016/j.jconrel.2018.10.009
27. LWC H, Liu Y, Han R, Bai Q, Choi CHJ. Nano-cell interactions of non-cationic bionanomaterials. *Acc Chem Res*. 2019;52(6):1519–1530. doi:10.1021/acs.accounts.9b00103
28. Ryu JH, Messersmith PB, Lee H. Polydopamine surface chemistry: a decade of discovery. *ACS Appl Mater Interfaces*. 2018;10(9):7523–7540. doi:10.1021/acsami.7b19865
29. Wang JL, Hu XY, Han CG, Hou SY, Wang HS, Zheng F. Lanthanide complexes for tumor diagnosis and therapy by targeting sialic acid. *ACS Nano*. 2022;16(9):14827–14837. doi:10.1021/acsnano.2c05715
30. van de Wall S, Santegoets KCM, Van houtum EJH, Bull C, Adema GJ. Sialoglycans and siglecs can shape the tumor immune microenvironment. *Trends Immunol*. 2020;41(4):274–285. doi:10.1016/j.it.2020.02.001

31. Zhou Z, Liu Y, Zhang M, et al. Size switchable nanoclusters fueled by extracellular ATP for promoting deep penetration and MRI-guided tumor photothermal therapy. *Adv Funct. Mater*. 2019;29(39):1904144. doi:10.1002/adfm.201904144
32. Kim A, Suzuki M, Matsumoto Y, Fukumitsu N, Nagasaki Y. Non-isotope enriched phenylboronic acid-decorated dual-functional nano-assembles for an actively targeting BNCT drug. *Biomaterials*. 2021;268:120551. doi:10.1016/j.biomaterials.2020.120551
33. Kim YH, Min KH, Wang Z, et al. Development of sialic acid-coated nanoparticles for targeting cancer and efficient evasion of the immune system. *Theranostics*. 2017;7(4):962–973. doi:10.7150/thno.19061
34. Wang H-X, Zuo Z-Q, Du J-Z, et al. Surface charge critically affects tumor penetration and therapeutic efficacy of cancer nanomedicines. *Nano Today*. 2016;11(2):133–144. doi:10.1016/j.nantod.2016.04.008
35. Ramasamy T, Ruttala HB, Gupta B, et al. Smart chemistry-based nanosized drug delivery systems for systemic applications: a comprehensive review. *J Control Release*. 2017;258:226–253. doi:10.1016/j.jconrel.2017.04.043
36. Xu X, Ho W, Zhang X, Bertrand N, Farokhzad O. Cancer nanomedicine: from targeted delivery to combination therapy. *Trends Mol Med*. 2015;21(4):223–232. doi:10.1016/j.molmed.2015.01.001
37. Lin X, Xiang X, Hao L, et al. The role of aurora-A in human cancers and future therapeutics. *Am J Cancer Res*. 2020;10(9):2705–2729.
38. Zheng D, Li J, Yan H, et al. Emerging roles of aurora-A kinase in cancer therapy resistance. *Acta Pharm Sin B*. 2023;13(7):2826–2843. doi:10.1016/j.apsb.2023.03.013
39. Wang X, Huang J, Liu F, et al. Aurora A kinase inhibition compromises its antitumor efficacy by elevating PD-L1 expression. *J Clin Invest*. 2023;133(9). doi:10.1172/JCI161929
40. Meulenbeld HJ, Mathijssen RH, Verweij J, de Wit R, de Jonge MJ. Danusertib, an aurora kinase inhibitor. *Expert Opin Investig Drugs*. 2012;21(3):383–393. doi:10.1517/13543784.2012.652303
41. Yuan CX, Zhou ZW, Yang YX, et al. Danusertib, a potent pan-aurora kinase and ABL kinase inhibitor, induces cell cycle arrest and programmed cell death and inhibits epithelial to mesenchymal transition involving the PI3K/Akt/mTOR-mediated signaling pathway in human gastric cancer AGS and NCI-N78 cells. *Drug Des Devel Ther*. 2015;9:1293–1318. doi:10.2147/DDDT.S74964